DIODE-PUMPED SOLID STATE LASER BASED SENSORS FOR CONE PENETROMETER APPLICATIONS

FINAL REPORT

J.H. SHORTER,* J. WORMHOUDT,* C.E.KOLB * J.J. ZAYHOWSKI,†
B. JOHNSON† AND N. NEWBURY†

JANUARY 1997

U. S. ARMY RESEARCH OFFICE
4300 SOUTH MIAMI BOULEVARD
RESEARCH TRIANGLE PARK, NC 27709-2211

CONTRACT NUMBER
DAAH04-96-C-0003

*CENTER FOR CHEMICAL AND ENVIRONMENTAL PHYSICS
AERODYNE RESEARCH, INC.
BILLERICA, MA 01821
AND
†LINCOLN LABORATORY
MASSACHUSETTS INSTITUTE OF TECHNOLOGY
LEXINGTON, MA 02173-9108

REPORT DOCUMENTATION PAGE

Form Approved
OMB NO. 0704-0188

1. AGENCY USE ONLY *(Leave blank)*	2. REPORT DATE	3. REPORT TYPE AND DATES COVERED
	January 9, 1997	Final 1 Dec 95 - 1 Nov 96

4. TITLE AND SUBTITLE
Diode-Pumped Solid State Laser Based Sensors for Cone Penetrometer Applications

5. FUNDING NUMBERS
DAAH04-96-C-0003

6. AUTHOR(S)
J. Wormhoudt, J.H. Shorter and C.E. Kolb (ARI)
J.J. Zayhowski, B. Johnson and N. Newbury (MIT/LL)

7. PERFORMING ORGANIZATION NAMES(S) AND ADDRESS(ES)
Aerodyne Research, Inc.
45 Manning Road
Billerica, MA 01821

Lincoln Laboratory
MIT
244 Wood Street
Lexington, MA 02173-9108

8. PERFORMING ORGANIZATION REPORT NUMBER

9. SPONSORING / MONITORING AGENCY NAME(S) AND ADDRESS(ES)
U.S. Army Research Office
P.O. Box 12211
Research Triangle Park, NC 27709-2211

10. SPONSORING / MONITORING AGENCY REPORT NUMBER
ARO 35074.1-RT-ST1

11. SUPPLEMENTARY NOTES
The views, opinions and/or findings contained in this report are those of the author(s) and should not be construed as an official Department of the Army position, policy or decision, unless so designated by other documentation.

12a. DISTRIBUTION / AVAILABILITY STATEMENT
Approved for public release; distribution unlimited.

12 b. DISTRIBUTION CODE

13. ABSTRACT *(Maximum 200 words)*
Site characterization using cone penetrometers is required for efficient and thorough screening of explosives contaminated soils at Army facilities. This report documents a Phase I STTR investigation into a novel class of miniature laser devices for sensitive detection of pyrolysis products of explosives and other nitrogen-containing soil contaminants. The major products, nitric oxide (NO) and nitrogen dioxide (NO_2), are detectable by laser-induced fluorescence (LIF) in the ultraviolet (UV) and visible spectral regions. Previous optical fiber-based systems cannot be applied to NO LIF due to poor fiber transmission in the UV. We investigated a detection system based on a diode-pumped microchip laser. This has the advantage that a near-infrared pump laser can be located on the surface, and efficiently transmitted over a fiber to crystals in the penetrometer probe which generate the Nd:YAG laser wavelength (1064 nm) and its harmonics. In Phase I we generated fifth harmonic UV light, and demonstrated detection of NO_2 fluorescence excited by 532 nm (second harmonic) light. We calculate that coatings can be fabricated which suppress laser oscillation at 1064 nm and allow operation at 1074 nm, whose fifth harmonic at 214.8 nm will overlap the NO absorption band. In Phase II we will fabricate this laser and develop and demonstrate a detection system.

14. SUBJECT TERMS	15. NUMBER IF PAGES
NO_x, nitrogen oxides, nitric oxide, nitrogen dioxide, cone penetrometers, soil contaminants, explosives contamination, energetic materials	21
	16. PRICE CODE

17. SECURITY CLASSIFICATION OR REPORT	18. SECURITY CLASSIFICATION OF THIS PAGE	19. SECURITY CLASSIFICATION OF ABSTRACT	20. LIMITATION OF ABSTRACT
UNCLASSIFIED	UNCLASSIFIED	UNCLASSIFIED	UL

TABLE OF CONTENTS

LIST OF ILLUSTRATIONS

LIST OF TABLES

1. Statement of the Problem

The Department of Defense (DOD) and the Department of Energy (DOE) are faced with the monumental task of cleaning up large tracts of military and nuclear weapons facilities which have sustained significant levels of soil and ground water pollution during this century. Explosive and energetic materials, including TNT, RDX and HMX, are pollutants of particular concern for the DOD. The department has a number of bases, munitions plants, storage depots and other facilities which have had extensive exposure to these toxic materials. In order to determine the extent of soil and ground water contamination and to assess the effectiveness of remedial actions, accurate and facile in situ detection systems for mapping and quantifying the subsurface distributions of explosives must be developed. In order to meet this need the government has initiated a tri-service site characterization and analysis penetrometer system (SCAPS) development program under the overall leadership of the Army Engineer Waterways Experiment Station (WES). The Department of Energy and the Environmental Protection Agency (EPA) have similar technology development programs underway [Bowders and Daniel, 1994].

The Army, Navy and Air Force have cooperated in the development of various sensors for specific classes of contaminants, including laser-induced fluorescence probes for hydrocarbon contaminants [Cespedes, et al., 1994] and a probe which senses the products of the pyrolysis of explosives [Cespedes, et al., 1995]. The latter device includes an electrochemical sensor which can detect NO and some other products of thermal decomposition of energetic materials, and a pyrolyzer unit. Subsurface NO_2 and NO (NO_x), identifying pyrolysis products of subsurface energetics contaminants such as TNT, RDX and HMX [Wormhoudt, et al., 1996], may also be detected by fluorescence techniques. NO_2 fluoresces when excited by visible light (600 - 400 nm) while NO fluoresces in the mid-ultraviolet (223-200 nm). Current fluorescence schemes for hydrocarbon detection utilize an above-ground pulsed UV laser source and deliver the interrogating laser pulse to the subsurface detection region via an optical fiber. Unfortunately, currently available optical fibers have relatively poor UV transmission characteristics. They will have difficulty delivering sufficient UV radiation for NO fluorescence, to ensure adequate detection levels [Davis, 1995]. An alternative approach, developed at MIT's Lincoln Laboratory, uses multi-mode silica fiber, developed for telecommunications applications, to transmit near infrared diode laser radiation to a subsurface set of nonlinear optical crystals. These crystals efficiently convert the pump photons into visible and/or UV laser pulses with wavelengths selected for efficient detection of subsurface contaminants. Lincoln Laboratory (LL) and MIT Department of Civil and Environmental Engineering (DCEE) researchers are already demonstrating the utility of this novel laser probe technology to detect subsurface petroleum derived aromatic compounds, including the BTEX species, using 266 nm radiation derived from the fourth harmonic of a diode-pumped fiber-coupled Nd:YAG 1064 nm laser.

2. Summary of Results

2.1 Phase I Technical Objectives

The goal of the Phase I project was to demonstrate the utility of a novel class of miniature laser devices in the sensitive detection of pyrolysis products of energetic materials in soils sampled by a cone penetrometer. These laser systems consist of a near-infrared diode laser pump, which would remain on the surface, and a series of small crystals which convert the pump light into infrared, visible and ultraviolet wavelengths. These crystals are packaged into a stainless steel cylinder which can easily be inserted into a cone penetrometer tube, and is connected to the pump laser with inexpensive silica fibers. The central objective of the Phase I work has been to interface laser systems developed at MIT Lincoln Laboratory (LL) with test apparatus constructed at Aerodyne Research (ARI) to make quantitative sensitivity measurements and demonstrate the feasibility of the approach. The following tasks were listed in the Phase I proposal:

1. Assemble a diode-pumped doubled Nd:YAG system providing 532 nm light for NO_2 resonance fluorescence detection; (LL)

2. Investigate laser systems based on 5th harmonic generation, beginning with the 1.064 μm Nd:YAG line, with the goal of developing a system which provides light near 215 nm for NO resonance fluorescence detection; (LL)

3. Interface LL laser systems with a fluorescence detection cell and a contaminated soil pyrolysis test apparatus; (ARI)

4. Demonstrate detection of NO_2 from pyrolysis of TNT/RDX contaminated soils, evaluate interferences and detection sensitivity, and investigate use of pump laser light as an alternative to hot filament pyrolysis; (ARI/LL)

5. Evaluate detection limits of fluorescence excited by 5th harmonic ultraviolet light; (ARI/LL)

6. Evaluate components of fluorescence collection/detection/signal processing system suitable for cone penetrometer applications (ARI).

In Phase I we demonstrated the feasibility of detecting the pyrolysis products, NO and NO_2, from explosives contaminated soils. A technical challenge in the Phase II program will be the design of a microchip laser system for supplying 215 nm light for NO detection. In Phase I, we demonstrated the production of the 5th harmonic of 1.064 nm (213 nm) and our calculations indicate that it will be possible to achieve 215 nm light by using the appropriate coatings on the crystals. The research at Lincoln Laboratories has also been very successful in producing 532 nm laser systems. In Phase I, we demonstrated the detection of ppm levels of NO_2 in a simple fluorescence cell. A theoretical analysis suggested that further improvements in Phase II should extend the detection limit to the ppb regime. After Phase I work began, the question of the feasibility of microchip laser heating of soil assumed greater importance, as the hot filament used for pyrolysis in the current WES probe became identified as a potential safety issue. This led us to defer an experimental component of Task 5 and most of the work on Task 6 until Phase II, and substitute some initial experiments on laser heating, which will also be discussed in this report.

2.2 Generation of 532 nm Light and Investigation of 5th Harmonic Generation (tasks 1 and 2)

Passively Q-Switched Microchip Lasers

Fiber-pumped passively Q-switched microchip lasers [Zayhowski and Dill, 1994; Zayhowski, 1995] are constructed by bonding a thin, flat wafer of gain medium (Nd^{3+}:YAG) to a thin, flat wafer of solid-state saturable absorber (Cr^{4+}:YAG). The composite structure is dielectrically coated and diced into small pieces, creating laser cavities that are typically 1 mm long and 1 mm across. The device is completed by bonding this laser cavity to the end of a multimode optical fiber, as shown in Figure 1. A diode laser coupled to the opposite end of the fiber provides the optical power to pump the device.

The principle behind the operation of a passively Q-switched laser is that the intracavity saturable absorber prevents the onset of lasing until the average inversion density within the cavity, N_0, reaches a value of

$$N_o = \frac{\gamma_{sat,rt} + \gamma_{par,rt} + \gamma_{op}}{\sigma l_{rt}} ,$$

where σ is the emission cross section at the lasing wavelength, l_{rt} is the round-trip path length of light within the cavity, $\gamma_{sat,rt} = -\ln(1 - \Gamma_{sat,rt})$ is the round-trip saturable loss constant, $\Gamma_{sat,rt}$ is the round-trip saturable loss, $\gamma_{par,rt} = -\ln(1 - \Gamma_{par,rt})$ is the round-trip unsaturable intracavity parasitic loss constant, $\gamma_{par,rt}$ is the round-trip unsaturable intracavity parasitic loss, $\gamma_{op} = -\ln(1 - \Gamma_{op})$ is the output coupling loss constant, and Γ_{op} is the transmission through the output coupler. The onset of lasing, at this point, produces a high intracavity optical field which quickly saturates the saturable component of the loss, increasing the cavity Q and resulting in a Q-switched output pulse.

If the cross section of the saturable absorber ($\sigma_{sat} = \gamma_{sat,rt} / N_{sat} l_{rt}$, where N_{sat} is the average density of saturable absorber sites within the cavity) is much greater than the cross section of the lasing transition, the change in the cavity Q can be modeled as instantaneous [Szabo and Stein, 1965]. In this case, the resulting pulsewidth is [Zayhowski and Kelley,1991;1993].

$$t_w = \frac{S_p t_{rt}}{\gamma_{sat,rt}} \left[\frac{\delta (1 + \delta)\eta}{\delta - \ln(1 + \delta)} \right] ,$$

where S_p is the pulse shape factor (typically $S_p = 0.86$ for Q-switched laser pulses), t_{rt} is the round-trip time of light within the laser cavity, η is the energy extraction efficiency of the laser pulse given by the implicit relationship $\eta (1 + \delta) = -\ln(1 - \eta)$, and $\delta = \gamma_{sat,rt} / (\gamma_{par,rt} + \gamma_{op})$ is the ratio of saturable to unsaturable cavity losses. For a given amount of saturable loss, the pulsewidth asymptotically approaches its minimum value of $t_w = 4 S_p t_{rt} / \gamma_{sat,rt}$ in the limit of large unsaturable losses ($\gamma_{par,rt} + \gamma_{op} >> \gamma_{sat,rt}$). However, this minimum pulsewidth is obtained at the expense of high threshold and low efficiency. In the opposite limit ($\gamma_{par,rt} + \gamma_{op} << V_{sat,rt}$) the pulsewidth asymptotically approaches $t_w = S_p t_{rt} / \gamma_{par,rt}$, the threshold of the laser is reduced, and the extraction efficiency is high. The best compromise between pulsewidth, threshold, and efficiency will depend on the application of the laser.

ULTRAVIOLET MICROCHIP LASER

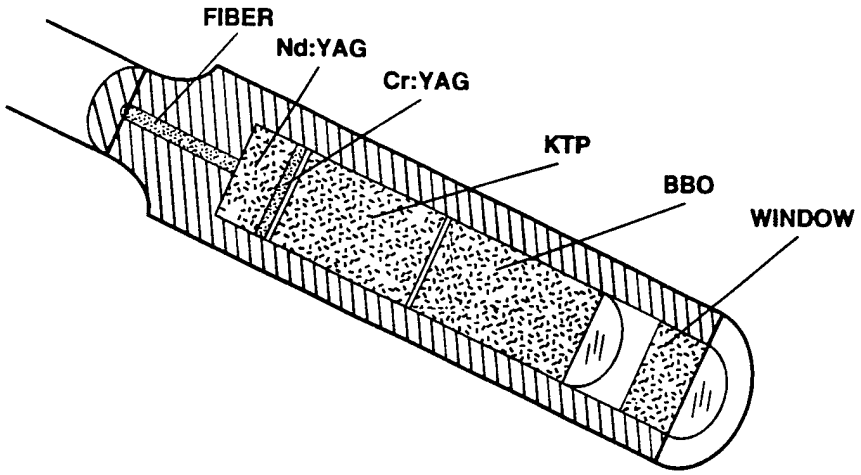

Figure 1. Schematic of a ultraviolet microchip laser

At pump powers well in excess of threshold, the period between the output pulses of a cw-pumped laser is approximately:

$$t_p = \frac{\tau P_{abs,thresh}}{P_{abs}} ,$$

where τ is the spontaneous lifetime of the gain medium, P_{abs} is the total amount of pump power absorbed within the lasing mode volume, and $P_{abs,thresh}$ is the pump power required to reach the threshold inversion density.

Generation of 1.064-μm Harmonics

The Q-switched microchip laser used for the initial demonstration of harmonic generation had a total cavity length of 1.25 mm, comprising 1 mm of 1.8 at.% Nd^{3+}:YAG and 0.25 mm of Cr^{4+}:YAG ($\gamma_{sat,rt} = 0.3$), and an output coupler with 85% reflectivity. It generated 8-μJ 440-ps pulses at a repetition rate of 10 kHz. The output at 1.064 μm was single frequency and diffraction limited, with a 6.8-mrad single-sided divergence and a $1/e^2$ waist diameter of 100 μm. It is the high peak power and ideal beam quality (diffraction-limited TEM_{00} transverse mode; transform-limited single longitudinal mode; linearly polarized) of the passively Q-switched infrared microchip laser that allow for efficient frequency conversion to the visible and UV regions of the spectrum using nonlinear optical crystals.

The 1.064-μm radiation from this microchip laser was frequency doubled with 44% energy efficiency in a 5-mm-long crystal of KTP placed adjacent to the laser (with no intervening optics) and oriented for type-II phase matching. The 532-nm output had a circularly symmetric, nearly Gaussian (super-Gaussian) profile with a 5.9-mrad divergence and an 85-μm waist diameter. The 3.5-μJ green pulses had a duration of 380 ps.

To generate the UV harmonics of the microchip laser output, we used antireflection-coated pieces of BBO (β-BaB_2O_4) oriented for type-I phase matching [Zayhowski, 1996]. In all cases, the crystals were 5 mm long, had flat faces, and were placed in the output path of the laser with no intervening optics. Before discussing the experimental UV generation, we will briefly review the theory of harmonic generation in BBO, in the limit of low conversion efficiency.

BBO has significant double refraction. For third, fourth, or fifth harmonic generation of the output of the Nd:YAG microchip laser, the harmonically generated beam walks out of the aperture defined by the generating beams in a length that is short compared to the length l of BBO used. The "aperture length" for coherent interaction of the beams is [Boyd, et al. 1965]

$$l_a = \frac{\sqrt{\pi}\,\omega_{e3}}{\tan(\rho_3)}$$

Here

$$\omega_{e3} \approx \left(\frac{1}{\omega_{e1}^2} + \frac{1}{\omega_{e2}^2} \right)^{-1/2} ,$$

in which ω is the $1/e^2$ radius of a nearly Gaussian beam, the subscripts 1, 2, and 3 refer to the generating and generated beams, respectively, and the subscript e indicates that the waist dimensions are measured in the direction perpendicular to the ordinary optic axis of the crystal (o is used to indicate the direction parallel to the ordinary axis); and the walk-off angle ρ_3 is given by

$$\tan(\rho_3) = \frac{\left(\frac{n_{o3}^2}{n_{e3}^2} - 1 \right) \tan\theta}{1 + \left(\frac{n_{o3}^2}{n_{e3}^2} \right) \tan^2\theta}$$

where n_{o3} and n_{e3} are the ordinary and extraordinary refractive indices at the frequency of the generated beam and θ is the phase-matching angle in the crystal defined by

$$\Delta k = 2\pi \left[\frac{n_{e3}(\theta)}{\lambda_3} - \frac{n_{o2}}{\lambda_2} - \frac{n_{o1}}{\lambda_1} \right] = 0 ,$$

with λ being the free-space wavelength and

$$n_{e3}(\theta) = \left(\frac{\cos^2 \theta}{n_{o3}^2} + \frac{\sin^2 \theta}{n_{e3}^2} \right)^{-1/2} .$$

The peak intensity of the generated beam is given by

$$I_3 = \frac{2\pi^2 d_{eff}^2}{n_{o1} n_{o2} n_{e3}(\theta) c \varepsilon \lambda_3^2} f(\delta\theta_1) f(\delta\theta_2) l_a^2 I_1 I_2 ,$$

where

$$d_{eff} = d_{31} \sin(\theta + \rho_3) - d_{22} \cos(\theta + \rho_3) \sin 3\phi$$

is the effective nonlinear coefficient ($\phi = 90°$ for a properly oriented crystal), c is the speed of light, ε is the dielectric constant of free space, and $f(\delta\theta) \leq 1$ is a function of the amount of power in one of the generating beams that falls within the acceptance angle of the crystal. When the acceptance angle of the crystal

$$\theta_{acc} = \frac{2\pi}{l_a} \left(\frac{\partial \Delta k}{\partial \theta} \right)^{-1}$$

is smaller than the divergence angle θ_e (in the BBO) of a generating beam, we will use

$$f(\delta\theta) \approx \frac{\theta_{acc}}{\theta_e} .$$

For all calculations, we will assume $|d_{31}| << |d_{22}|$, $|d_{22}| = 2.2$ pm/V [Eckardt, et al. 1990] and the refractive indices given in Table I below [Eimeral, et al. 1987].

Table I - Refractive Indices of BBO

λ	1064	532	355	266	213
n_o	1.54254	1.55552	1.57757	1.61461	1.67467
n_e	1.65510	1.67493	1.70556	1.75707	1.84707

The peak power P_3 and pulse energy E_3 in the generated beam are calculated from the peak intensity. In the dimension parallel to the ordinary axis of the BBO, we will assume that the generated beam has a nearly Gaussian profile with a $1/e^2$ radius of ω_{03}. In the orthogonal dimension, the direction of walk off, the profile is roughly top-hat, with a diameter

$$d_3 = \frac{l}{\tan(\rho_3)} \quad .$$

The peak power is approximately

$$P_3 = \frac{\sqrt{2}\, I_3}{\sqrt{\pi}\, \omega_{o3}\, d_3}$$

and, after accounting for the temporal shape of the pulse, the pulse energy is approximated by

$$E_3 = 1.16\, P_3\, t_3 \quad ,$$

where a reasonable estimate of the pulse duration (FWHM) is

$$t_3 = \left(\frac{1}{t_1^2} + \frac{1}{t_2^2} \right)^{-1/2} \quad .$$

The green output of the KTP was doubled to produce 266-nm UV radiation with 20% energy efficiency in a 5-mm-long crystal of BBO placed adjacent to the KTP. The far-field profile of the resulting 0.7-μJ UV pulses was nearly Gaussian in the dimension parallel to the ordinary axis of the BBO, with a $1/e^2$ single-sided divergence of 4.1 mrad. In the opposite dimension the far-field profile approximated a $\sin^2 x/x^2$ pattern, with an angular separation of 1.1 mrad between the two central nodes. The near-field and temporal profiles of the UV output were not measured.

From the theory presented above, for fourth-harmonic generation of the microchip output $\theta = 47.3°$, $\rho_3 = -4.84°$, $|d_{eff}| = 1.62$ pm/V, $\omega_{o3} = 30$ μm, $d_3 = 423$ μm, $t_3 = 269$ ps, $l_a = 627$ μm, $n_{e3}(\theta) = 1.687$, and $f(\delta\theta_1) = f(\delta\theta_2) = 0.91$. With $I_1 = I_2 = 287$ MW/cm^2 ($I_1 = \pi\, \omega_1^2\, P_1 / 2$), this gives calculated values of $I_3 = 17.9$ MW/cm^2, $P_3 = 2844$ W, and $E_3 = 0.89$ μJ; in excellent agreement with the 0.7 μJ obtained. From the theoretical calculations, the far-field divergence of a diffraction-limited beam in the direction parallel to the ordinary axis would be 2.8 mrad, indicating that the actual beam was ~1.4 times diffraction limited, similar to the 532-nm generating beam. In the opposite dimension, the far-field profile of a 423-μm-diameter top hat should have central nulls spaced by 1.2 mrad, in good agreement with the observed value.

The 266-nm radiation was also combined with the fundamental to generate the 5th harmonic of the Nd:YAG line. This 213-nm light is near coincident with NO absorption lines. When the crystals were aligned for maximum output energy, the ordinary axis of the fifth-harmonic crystal was perpendicular to the ordinary axis of the fourth-harmonic crystal, and fifth-harmonic pulse energies of ~ 0.01 μJ were obtained. The far-field profile of the 213-nm output is qualitatively similar to that of the 266-nm light, except rotated by 90° due to the relative orientations of the fourth- and fifth-harmonic crystals. The $1/e^2$ divergence in the nearly Gaussian dimension was ~1.5 mrad, and the central node spacing in the other dimension was 0.8 mrad.

Only half of the fundamental remaining after second-harmonic generation in the KTP is properly polarized to contribute to fifth-harmonic generation. The useful 1.064-μm radiation is polarized perpendicular to the ordinary axis of the BBO crystal used for fourth-harmonic generation, and experiences refraction in that crystal, with a "walk-off" angle of -4.03°. As a result, it overlaps the fourth-harmonic radiation at a position of uniform, maximum intensity. If

we ignore the divergence of the 1.064-μm radiation, the theory presented above predicts a pulse energy of 0.01 μJ. At the position of the fifth-harmonic crystal, the fundamental beam should have diverged by 40% in radius, decreasing the amount of generated fifth harmonic proportionally.

The most thoroughly tested of the devices discussed above is a frequency-quadrupled passively Q-switched microchip laser. The laser and the nonlinear crystals are packaged in a stainless-steel cylinder 1 cm in diameter by 3 cm in length. [Zayhowski, et al. 1995]. As a result of the short aperture length (l_a) in the BBO, the temperature window for UV generation is large and at least 1 mW of time-averaged UV output is obtained over a temperature range from 0 to 70° C. Currently, this device has been operated for $>10^{10}$ shots without degradation.

The use of 5-mm-long crystals of BBO in all of the experiments described above is somewhat arbitrary. When the aperture length in the nonlinear crystal is short compared to the crystal length, as is the case here, the conversion efficiency is linearly dependent on the crystal length, to the extent that pump depletion and beam divergence can be neglected. The amount of UV generated at any of the Nd:YAG harmonics could be increased simply by using a longer piece of BBO. Since the acceptance angle and temperature window for nonlinear conversion are determined by the aperture length, they are not affected.

Generation of 215-nm Radiation

Strong NO absorption bands occur at wavelengths between 214.5 and 215.5 nm. Since submitting our Phase I proposal we have successfully demonstrated [Zayhowski, 1996] up to 1 mW of 213-nm light, from the 1.064-μm Nd:YAG laser line. This 5th harmonic light falls slightly outside of the desired wavelength region, but established that sufficient levels of 5th harmonic can be generated using the microchip design, thus fulfilling an important part of our Phase I, Task 2. There is another Nd:YAG fluorescence line centered at 1.074 μm, whose fifth harmonic at 215 is well matched to the NO absorption. The peak cross section of Nd:YAG at 1.074 μm is about one half the cross section at 1.064 μm. With properly designed dielectric coatings on the microchip lasers, it should be possible to suppress the 1.064-μm line and operate a passively Q- switched device at 1.074 μm. There is no significant change in the properties of the saturable absorber (Cr:YAG) or the nonlinear crystals required for fifth-harmonic generation (KTP and BBO) as the fundamental wavelength is shifted from 1.064 to 1.074 μm.

An initial design for a passively Q-switched 1.074-μm microchip laser would comprise 1 mm of 1.8 at.% Nd^{3+}:YAG and 0.125 mm of Cr^{4+}:YAG ($\gamma_{sat,rt} = 0.15$), and an output coupler with 93% reflectivity at 1.074-μm. To suppress oscillation at 1.064-μm, the product of the reflectivities of the pump-side coating and the output coupler would have to be less than 60% at that wavelength, while still maintaining a pump-side coating reflectivity of greater than 99.5% at 1.074-μm. To accomplish this, the output coating would be designed as a narrow-pass optical filter centered at 1.064-μm; the bandwidth and transmission of the filter would be selected to give the proper reflectivity at 1.074-μm. The theoretical performance of such a coating is shown in Figure 2; the fabrication of the coating will be challenging, but should be possible. The pump-side coating will be the same as the one used for the 1.064-μm device.

A 1.074-μm microchip laser fabricated according to the above specifications should operate at the same pulse repetition rate as the 1.064-μm device discussed earlier in this proposal, 10 kHz, with comparable time-averaged power and pulse energy. Because of the decreased gain cross section, the pulses should be twice as long and the peak powers half as large. The reduced peak power will reduce the efficiency $\eta_{n,\lambda}$ of the nonlinear frequency conversion by

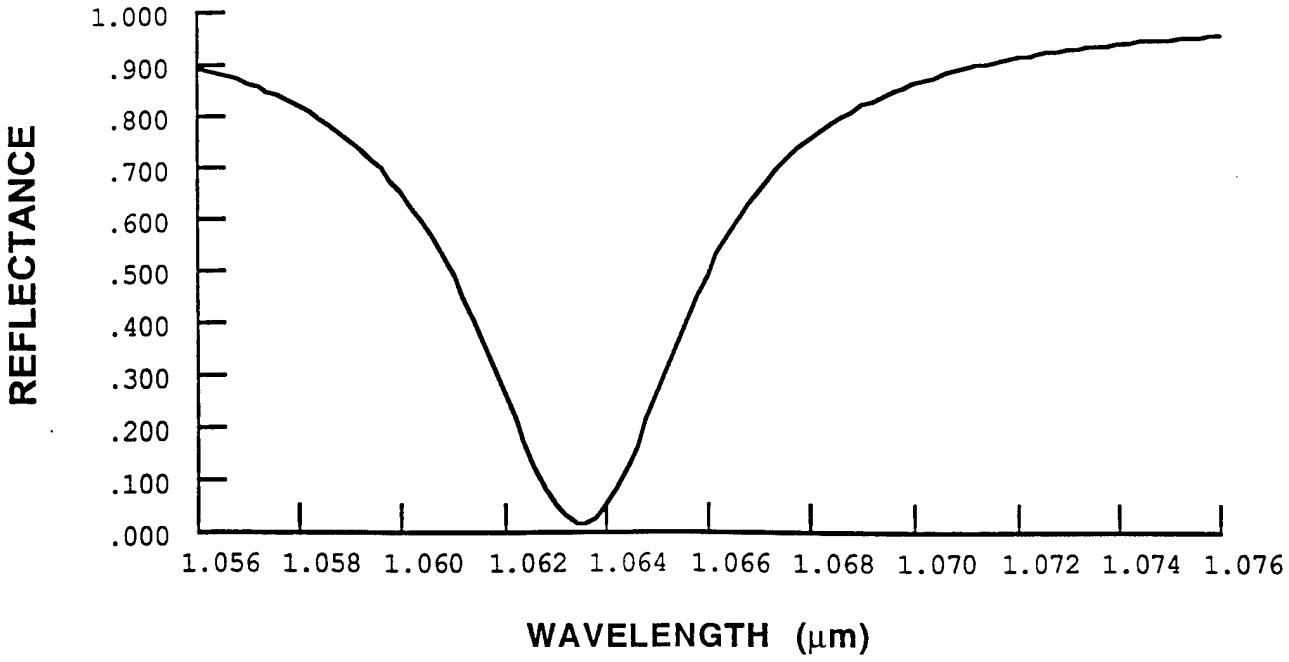

Figure 2 Theoretical performance of a coating for 1.074 μm

$$\frac{\eta_{n,1.974}}{\eta_{n,1.064}} \equiv \frac{E_{1.074/n}}{E_{1.064/n}} = \frac{t_{w,1.074}}{t_{w,1.064}} \left(\frac{P_{1.074}}{P_{1.064}} \right)^n ,$$

where n is the order of the harmonic and we have assumed that we are not saturating the harmonic conversion efficiency for either fundamental wavelength. For fifth-harmonic generation (n = 5) at 1.074 μm, with $P_{1.074} = 0.5P_{1.064}$ and $t_{w,1.074} = 2t_{w,1.064}$, we would expect the pulse energy to be reduced by a factor of 16 relative to the amount demonstrated at 213 nm. This corresponds to 0.6 nJ/pulse, for a time-averaged power of 6 μW. Since we are strongly saturating the second harmonic generation with the 1.064-μm radiation, we expect to do about two times better than this, to obtain in excess of 12 μW of 215-nm radiation.

Further improvements in the power of the 215-nm frequency-quintupled microchip laser can be obtained by improving the efficiency at the fundamental wavelength. Standard growth procedures do not allow the growth of Nd:YAG with Nd concentrations much in excess of 1.8 at.%; modern epitaxial techniques, however, will allow the custom growth of higher-concentration material. At 1.8 at.% Nd only about one third of the pump light is absorbed within the volume of the oscillating laser mode. If the Nd concentration were increased, the amount of pump light absorbed would also increase. The additional absorbed pump light could be used to increase both the repetition rate of the device and the peak power of the pulse. Any increase in peak power would pay off manyfold in harmonic generation.

The minimum pulse width of a microchip laser is nearly proportional to $1/\rho\tau$, where ρ is the concentration of Nd and τ is the upper-state lifetime of the Nd:YAG. The pulse energy is

proportional to $\rho\tau$. The peak power is therefore proportional to $(\rho\tau)^2$. At the same time, the increased absorption coefficient (proportional to ρ) would increase the pulse repetition rate in proportion to $1/\tau$. The amount of time-averaged fifth harmonic generated is therefore proportional to $\rho^9\,\tau^8$. The upper-state lifetime in Nd:YAG is dependent on the Nd concentration and is roughly accounted for by

$$\tau = \frac{\tau_o}{1 + \left(\rho \,/\, \rho_{cq}\right)^2} \quad ,$$

where τ_0 is the lifetime of the upper state at arbitrarily low Nd concentrations and ρ_{cq} = 2.63 at.% for Nd in YAG. The maximum time-averaged fifth harmonic is therefore obtained for $\rho = (9/7)^{1/2}\,\rho_{cq}$ = 3 at.%. This can be grown using epitaxial techniques, and would improve the amount of 215-nm light generated by 2.7 compared to the use of 1.8 at.% Nd, resulting in over 30 μW of power.

Higher 215-nm powers would require a higher-power pump source. A 10-W diode-laser pump should result in powers well in excess of 1 mW, in a device that could still be packaged to fit within the 1-inch bore of a cone penetrometer.

2.3 Assembly of Phase I Fluorescence Cell

A small fluorescence cell for Phase I demonstration of NO_2 detection was constructed at ARI. As seen in Figure 3, a simple arrangement was designed which allowed us to incorporate common components, including a photomultiplier tube (PMT) already available at Aerodyne, and windows and filters available from manufacturers' stock. The simple fluorescence cell design also has an easily characterized fluorescence collection geometry.

The fluorescence cell was designed to mount to the PMT housing via an adapter flange. The cell was constructed of stainless steel and coated on the interior with flat black paint to minimize laser scatter. The photocathode of the PMT (Hamamatsu R955) is 8 mm x 24 mm. Because the PMT side-arm of the cell has a 1.9 cm i.d., the viewing region of the PMT is 8 mm x 1.9 mm. Collection optics are not used to collect the NO_2 fluorescence, in keeping with maintaining simplicity of design. A bandpass filter at 700 ± 25 nm (Corion, S25-700-F) is mounted in front of the PMT to minimize interference from laser scatter and room lights. This filter was chosen to transmit the NO_2 fluorescence which occurs in three regions between 615 and 775 nm [Schofield, 1997] (see section 2.4). The peak transmission of the filter is 50%. As will be discussed in section 2.4, other filter arrangements would improve the transmission of the fluorescence to the detector. The microchip laser assembled by LL in task 1 provides the 532 nm excitation energy for NO_2 laser induced fluorescence. The laser is transmitted through the cell in a path perpendicular to the side-arm for the PMT, passing through windows mounted at Brewster angles. The windows are 1/16" thick S1-UV and transmit ~100% of light in the 0.28 to 2.0 μm region. There is also a window of this material between the cell and the PMT.

The cell was operated with sample gas flowing through the cell at atmospheric pressure. The cell is designed to also allow measurements at reduced pressure. A port for a pressure gauge is provided.

The fluorescence cell was used in experiments to detect NO_2 at varying mixing ratios, as will be described in subsection 2.4. The design is simple and provides a characterizable collection system. Laser scatter was found to be negligible and the PMT is fairly insensitive to the exact alignment of the laser through the cell, provided it passes cleanly through the cell.

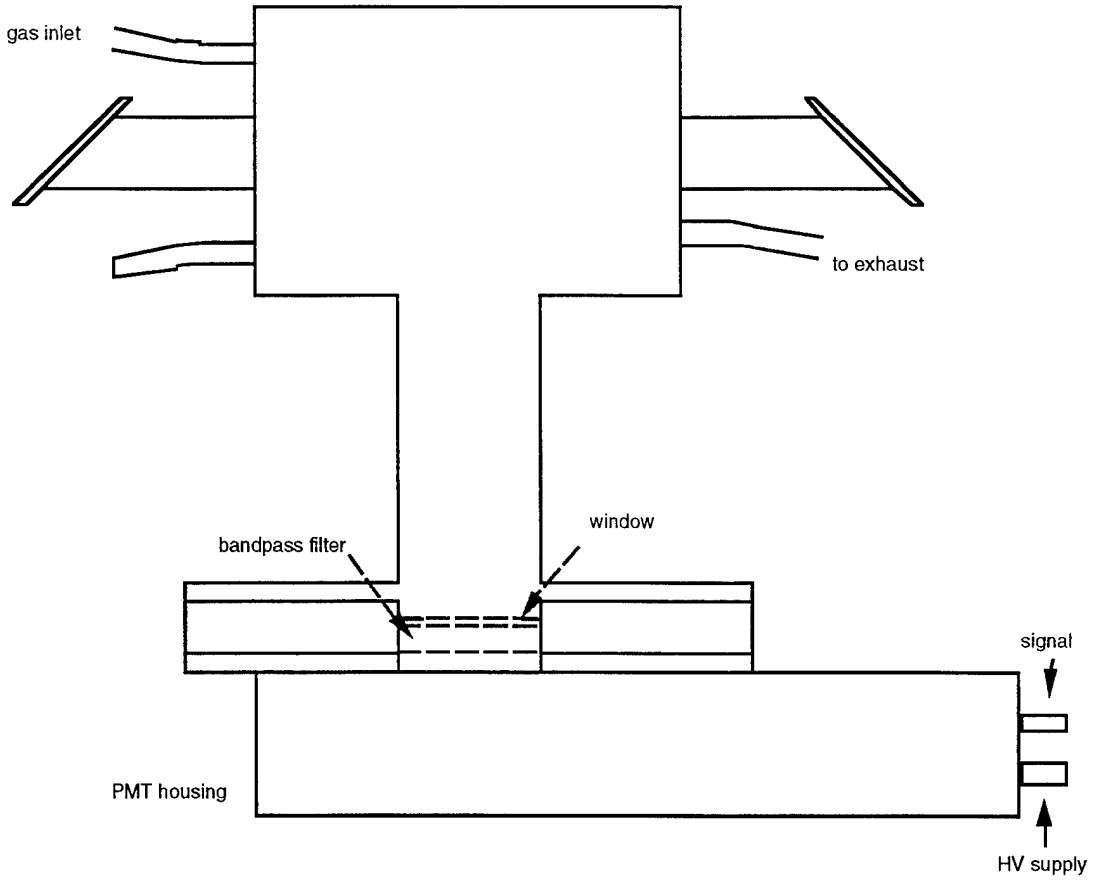

Figure 3. Fluorescence cell mounted on PMT housing.

2.4 Demonstration of NO_2 Detection and Evaluation of Detection Sensitivity

The overall goal of this task was to demonstrate the detection of NO_2 produced in the pyrolysis of energetic materials in soils, using the Phase I fluorescence cell. A straightforward, alternate approach involves filling the fluorescence cell with known amounts of the target gas and measuring fluorescence signals. We chose this method because we know from previous experiments that NO_2 is indeed a pyrolysis product. In our ongoing work for the Waterways Experimental Station (WES), we have detected NO_2 and NO from TNT and RDX contaminated soils that are sufficiently heated. NO and NO_2 emitted from heated 100 ppm_{wt} TNT in dirt is shown in Figure 4. In this experiment the heating element was a planar heater with the heater wire wrapped in a spiral below a disk of machinable ceramic. The ring shaped heating surface has a 2 cm o.d. and 0.6 cm i.d. The heater was operated at ~900C. NO_2 has also been detected upon heating of contaminated soil with a single filament at 900C.

A cylinder of 95.8 ppm NO_2 in N_2 (Scott Specialty Gases) served as our standard for the experiments. The mixing ratio was varied by diluting the standard with known amounts of zero air. NO_2 fluorescence was measured by flowing the standard, or dilutions, at atmospheric pressure through the fluorescence cell described in the previous section. The NO_2 is excited by the 532 nm light, the second harmonic of the Nd:YAG 1.064 μm line obtained from a microchip laser assembled at Lincoln Laboratory. The laser provided 1.3 μJ in a 380 psec pulse operating at 10 kHz. The NO_2 absorption spectrum in this region has many lines and at atmospheric pressure can be thought of as a quasi-continuum, albeit one with substantial spectral structure. The NO_2

fluorescence at ~700 nm was detected perpendicular to the laser path by a PMT, and the signal was averaged using a boxcar integrator (Stanford Research, SR250). A photodiode with a fast amplifier detected the small 532 nm reflection from the Brewster window on the inlet side of the cell. The photodiode signal served as the trigger for the boxcar. A 120 ns gate at zero delay was used to average 10k samples. At atmospheric pressure the fluorescence lifetime of NO_2 is ~100 psec. This is experimentally significant for several reasons. It necessitated the use of a fast photodiode in order to sample at zero delay, i.e., as soon as the laser pulse occurs. The lifetime is shorter than the pulse so the fluorescence is present for the duration of the pulse and any laser scatter cannot be discriminated from the signal in the time domain. The scattered light from the laser is, however, blocked from the PMT by the bandpass filter.

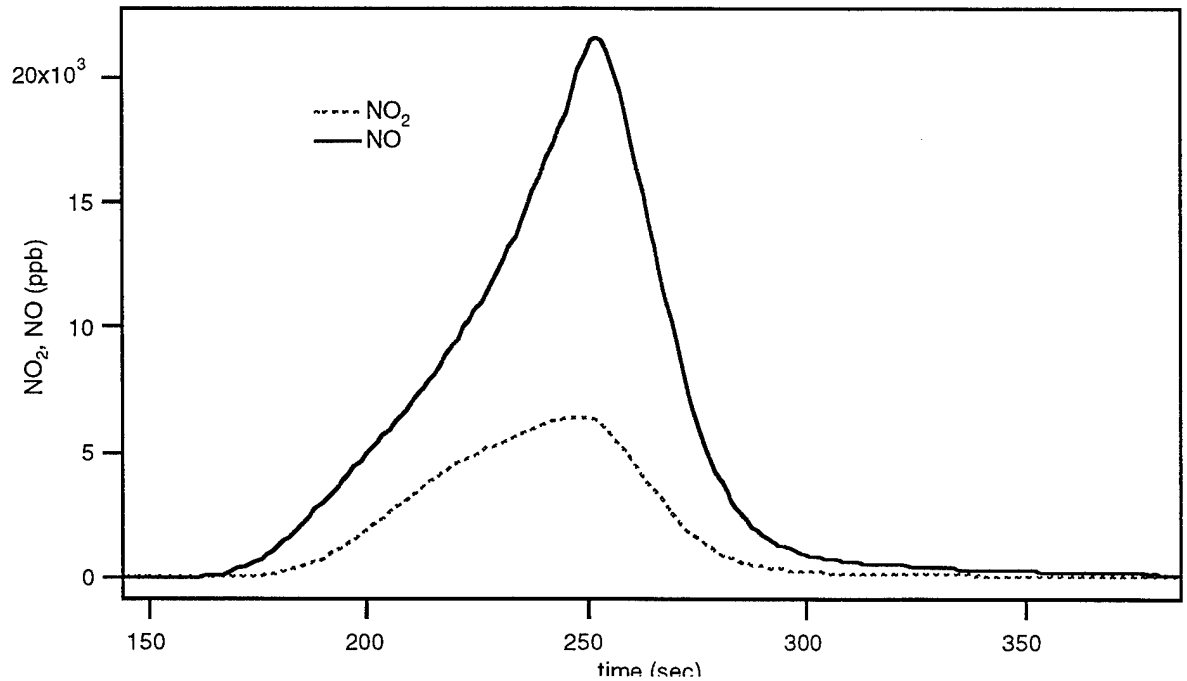

Figure 4. NO_2 and NO obtained from soil contaminated with 100 ppm_{wt} TNT with lab model of cone penetrometer sensor.

We estimate the NO_2 detection limit of our Phase I fluorescence detection system to be approximately 10 ppm. There are a number of ways to increase the signal level and to decrease the noise of the measurement. Although the total excitation pathlength of the laser in the cell is 14 cm, the pathlength within the field of view of the detector presently is only 1.9 cm. If a multipass cell with a 12 m pathlength, configured with detection to include all of the fluorescence, replaced the Phase I fluorescence cell, the signal intensity would be increased by ~600 times, as given by the expression for fluorescence signal on the next page. This is a reasonable pathlength for a miniature multipass cell for a SCAPS device. A more sensitive PMT in the 700 nm region would also improve our sensitivity to NO_2. The PMT used in the reported experiments has a quantum efficiency of 5% at 700 nm. This PMT was used because it was readily available at Aerodyne, has a reasonable coverage in the visible, and has good current amplification. PMTs with a higher efficiency at 700 nm, however, are available and will be incorporated into the prototype device. A factor of at least 2 to 3 in sensitivity should be gained here.

An experiment was also conducted to test the transmission of the 700 nm bandpass filter in front of the PMT. We found that the filter which is centered at 700 nm with a bandwidth (FWHM)

of 25 nm, transmits only ~10% of the total fluorescence from 532 nm excitation. There are 2 reasons for this. First, not all of the fluorescence occurs within the filter window. Schofield [Schofield, 1977] reports that for 546.1 nm excitation, the fluorescence occurs in the following three regions with corresponding relative intensities: 1.0 (615-670 nm), 1.01 (670-720), and 0.53 (720-775). A significant portion of the fluorescence is outside the bandwidth of the filter. Also, the exact fluorescence wavelengths for 532 nm excitation may be slightly different. The second reason for 10% transmission is that, although the peak transmission of the filter is 50%, much of the fluorescence within the window falls outside the peak transmission region. A different filter arrangement should be able to greatly improve the transmission of fluorescence to the PMT while still blocking scattered light from reaching it.

We estimate that we will be able to get about three orders of magnitude improvement in sensitivity with the above modifications to the detection system. This would bring the NO_2 detection limit to ~10 ppb. This will give us a very sensitive device. As shown in Figure 4, we measure much higher levels of NO_2 evolved from heating of contaminated soils.

An example of NO_2 fluorescence measurement is given in Figure 5. The signal from 95.8 ppm NO_2 drops to zero when the delay of the sampling gate is increased (2 μsec). The figure also shows the change in signal when the gas flow was switched from the standard to zero air. The fluorescence signal is also shown to be linearly dependent on the NO_2 mixing ratio in Figure 6. The NO_2 standard was diluted with zero air in these measurements. The precision of the NO_2 measurement will be greatly enhanced when the improvements to the optical system discussed above are implemented.

We have demonstrated both the generation of NO_2 from contaminants in soils using the Aerodyne Research test apparatus and its detection using the Phase I fluorescence cell. We have verified that interferences including laser scatter can be suppressed. We estimate a minimum sensitivity level for NO_2 of 10 ppb, after optimizing the optical cell design and components, based on our Phase I experimental results.

We can also compare the experimental fluorescence intensity with a calculated intensity which follow the estimation techniques used by Schofield [1977] combined with the actual experimental conditions. The spectroscopy of NO_2 at atmospheric pressure is not well understood. The NO_2 spectrum is so congested with lines, it can be thought of as a quasi-continuum with spectral structure. This makes analysis of its spectrum extremely difficult. The comparison of experimental and calculated intensity gives us a better understanding of the fluorescence upon which we can estimate the expected fluorescence signal from contaminated soils in our SCAPS device. We first present here a calculation of the fluorescence signal from 95.8 ppm NO_2 excited by 532 nm light and then compare it to our experimental result.

Schofield's expression for fluorescence signal is

$$I_f = \frac{\Omega_F \, f \, \Theta}{4\pi} \cdot \frac{k_f}{k_f + k_q[M]} \cdot I_s a_s \cdot n\sigma l$$

where factors for any decrease in the intensity of the exciting radiation between the source and field of view, or attenuation of the fluorescence before reaching the detector, have not yet been included.

In the first group of terms, the detector factor, Ω_F is the solid angle for fluorescence collection into the detector. In our present system the viewing region is 1.52 cm^2 and the collection solid angle fraction is 9.15×10^{-4}. The fraction of fluorescence that passes through the filter to the PMT was measured in the laboratory and found to be 0.09. This measurement takes

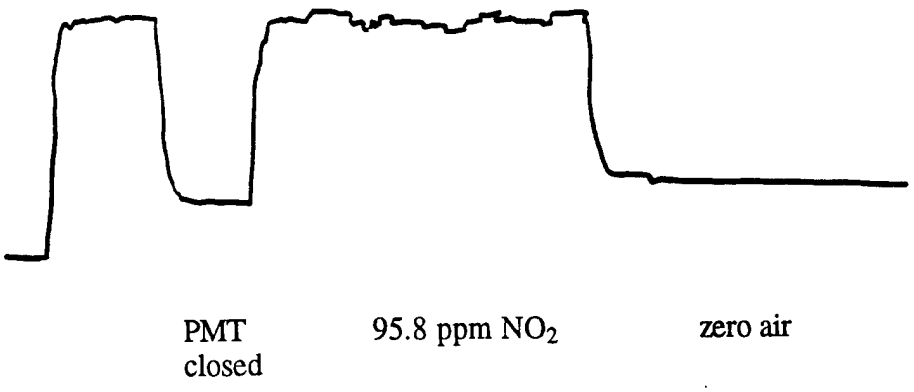

Figure 5. NO_2 fluorescence data for 95.8 ppm NO_2.

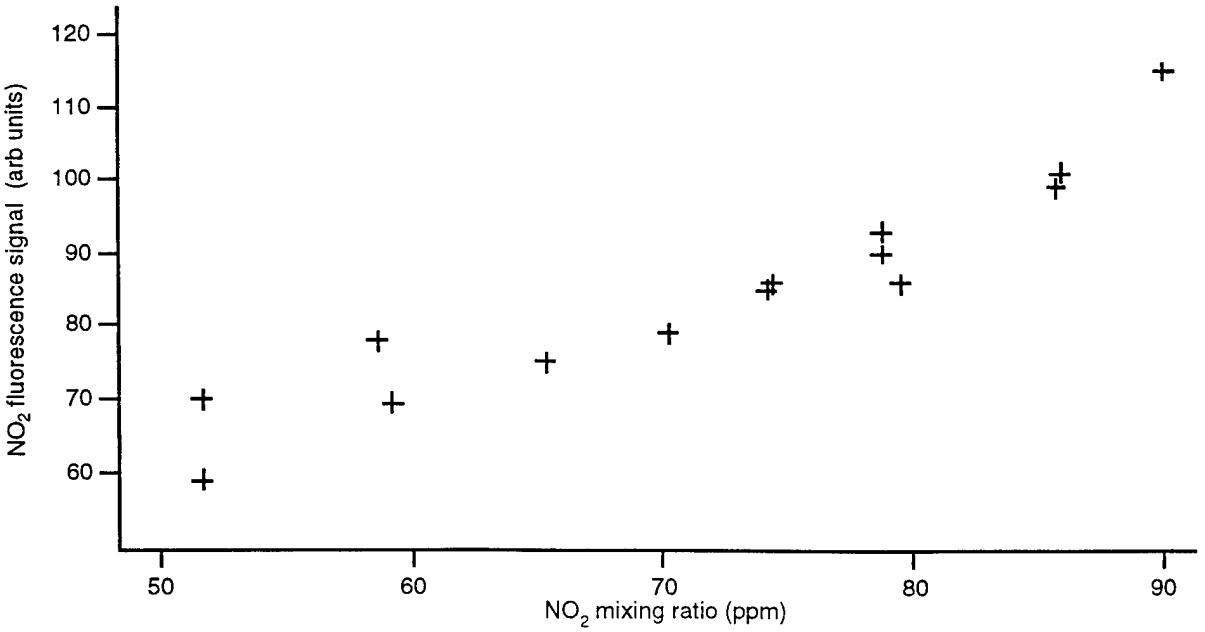

Figure 6. Fluorescence as a function of NO_2 mixing ratio

into account both the fraction of the fluorescence which lies within the bandpass of the filter, f, and the filter transmission, Θ. The measurement is consistent with the expected transmission of the filter (50% peak transmission), and the fluorescence region which is within the 25 nm FWHM bandwidth of the filter. The fraction of overlap of absorption with laser light is assumed to be 1 and the time gate was set long enough to include all of the fluorescence signal.

In the second term, the fluorescence efficiency factor, k_f is the radiative rate and $k_q[M]$ is the quenching rate. Using a radiative constant of 12540 s^{-1} [Patten, et al., 1990] and a quenching rate of 1.09 x 10^9 s^{-1} [Patten et al., 1990], we obtain 1.15 x 10^{-5} for the fluorescence efficiency factor. For the third term, the source factor, we use 1.3 μJ/pulse, the power of the 532 nm light from the microchip laser in our experiments. Finally, the absorption cross section of NO_2 at 532 nm, taken from Schofield, is 1.6 x 10^{-19} cm^2. In our experiment the pathlength, l, is 1.9 cm, and n, the density of NO_2 molecules, is 2.4 x 10^{15} cm^{-3}. From all of these terms we obtain I_f = 2.5 photons/pulse, or 7.1 x 10^{-19} J/pulse of 700 nm fluorescence. This is equal to 7.0 x 10^{-12} J/s for the observed 100 nsec signal of the detection arrangement of our experiment.

The PMT responsivity (radiant sensitivity x photocathode gain) was estimated as 2.4 x 10^5 A/W. This is based on the specification of the PMT at 700 nm and the supply voltage applied in the measurements. Our expected PMT response due to the fluorescence signal from 95.8 ppm NO_2 is 1.7 x 10^{-6} A. The observed experimental response was 2.0 x 10^{-7} A. The observed signal was 8.5 times lower than we expected, but we believe this is in reasonable agreement. The PMT, for example, is a number of years old and, since PMTs are known to degrade with time, probably no longer provides the expected gain. Because of the complexity of the NO_2 spectrum, there has also been some discrepancy or limited information in the literature with respect to the quenching rates for this fluorescence region.

2.5 Evaluation of 5th Harmonic UV source for NO Detection

Our Phase I work plan included an experimental task demonstrating ultraviolet fluorescence detection using the microchip laser. The goals and experimental work of this task will be similar to the NO_2 detection work described above, but it was decided that it was a less critical task than the added task of a first assessment of laser heating, described below, so it will not be addressed until early in the Phase II program. It is appropriate here to make a few comments about why it is less important that this task be completed before the Phase II program, and what issues remain in NO detection after NO_2 detection has been investigated.

Understanding the change in detection sensitivity for NO in a system whose sensitivity to NO_2 has already been characterized involves only a few factors, three of which are of key importance: 1) the difference in laser power; 2) the difference in fluorescence quenching (and thus, the efficiency with which excited NO can emit fluorescence), and 3) the absorption cross section. The powers of the green and ultraviolet laser beams have already been measured. Quenching rates are well documented for both NO and NO_2, so that an adequate estimate for the fluorescence efficiency can be made. Finally, the positions and absorption cross sections of NO lines are very accurately known, as is not the case for NO_2 where huge numbers of overlapped lines make analysis of its highly irregular spectrum extremely difficult. If we take the current situation of ultraviolet power levels lower than 532 nm power by a factor of 350, and also take into account an increase of 80 in the fluorescence efficiency factor and an increase of more than 50 in the absorption cross section, we expect that sensitivity to NO will be over an order of magnitude better than that for NO_2.

While the most important issues in detection sensitivity have been settled by our NO_2 observations and analysis, there will be useful work to be done at the more detailed level when we demonstrate UV fluorescence detection. For example, the issue of background fluorescence from surfaces may be different in the UV. Seeking the best match between laser and absorption line

widths may suggest operating the fluorescence cell at a reduced pressure. Finally, although we have no reason to suspect there will be a difficulty in setting up the laser to operate in exact coincidence with a strong absorption line of NO (the temperature tunability of the laser is larger than the NO line spacing), this must be demonstrated, and we must gain enough experience with the technology that we know it will not be a problem in a field instrument.

2.6 Evaluation of the Microchip Laser as a Pyrolysis Source for Explosives Detection

The current SCAPS explosives sensor, shown in Figure 7, utilizes as a heating element two turns of 0.010 in diameter platinum wire, wrapped around a ceramic sleeve on the outside of the penetrometer tube. When withdrawal of the penetrometer is begun, a sacrificial protective sleeve is left behind, revealing the heating wire, which is within 0.1 inch of the soil which forms the wall of the hole. The segments of the wire which do not contact the ceramic (thermal expansion results in some portions of the filament standing free from the penetrometer tube) are heated to about 900 °C. This results in some combination of heating of soil particles which contact the wire, and heating of particles which stand away enough from the bulk soil of the hole such that they can be easily heated by radiation from the wire. In the case of TNT, this heating only results in vaporization, not decomposition, of the TNT. The airflow out of and then into the probe (sweep air) moves this TNT vapor near enough to the hot filament that some of the vapor is thermally decomposed into small, more easily detectable molecules like NO. Other energetic materials, such as RDX, have lower vapor pressures but also decompose at lower temperatures and so may yield decomposition products directly from the condensed phases.

The hot filament method of soil heating has been observed to have some drawbacks. The filament breaks, and can become covered with mud. Concern has been expressed that the glowing filament might be a safety hazard. The WES personnel who operate the current probe have begun developing a lower temperature, more robust external heater, but it is not yet known if this will be practical. Furthermore, if rejection of background signals becomes a key issue and detection of several product molecules (like NO and NO_2) is shown to be a useful technique to discriminate against background interferences, the question must then be addressed as to whether thermal heating, or some other technique, results in the largest differences in product species between explosives and uncontaminated soils.

With these motivations, an attractive area of investigation in Phase II will be the possibility that the components of the microchip laser output can be used to perform soil heating. Among the possibilities are heating to current temperature levels, so that TNT is only vaporized, or heating smaller volumes to higher temperatures, so that TNT is decomposed in the soil. In the former case, a hot filament might still be required, but it could be smaller and in a much more protected position in the penetrometer probe. As regards the latter option, we know that heating to high temperature levels is possible since Lincoln Laboratories has demonstrated that a similar laser can be focused to yield a LIBS (Laser Induced Breakdown Spectroscopy) spark in a soil sample spiked with small aluminum chips. Determining whether a laser heating technique can be devised which has significant advantages and no major drawbacks in comparison to heating by a hot filament requires a quantitative understanding of the processes involved. Under our contract with WES, we have been developing heat transfer modeling to predict soil temperatures with various heating techniques. However, our knowledge of model parameters for soil is not good enough for our predictions to stand on their own. Instead, we must do some laboratory experiments and match model predictions to them in order to develop a trustworthy parameter set. For heating with various types of hot filaments, those experiments can include measurement of temperatures using fine wire or foil thermocouples embedded in the soil. For laser heating, the focal spot is typically much smaller than thermocouple beads, and the most useful experiments simply measure decomposition products evolved from laser irradiation of TNT. A schematic of these experiments

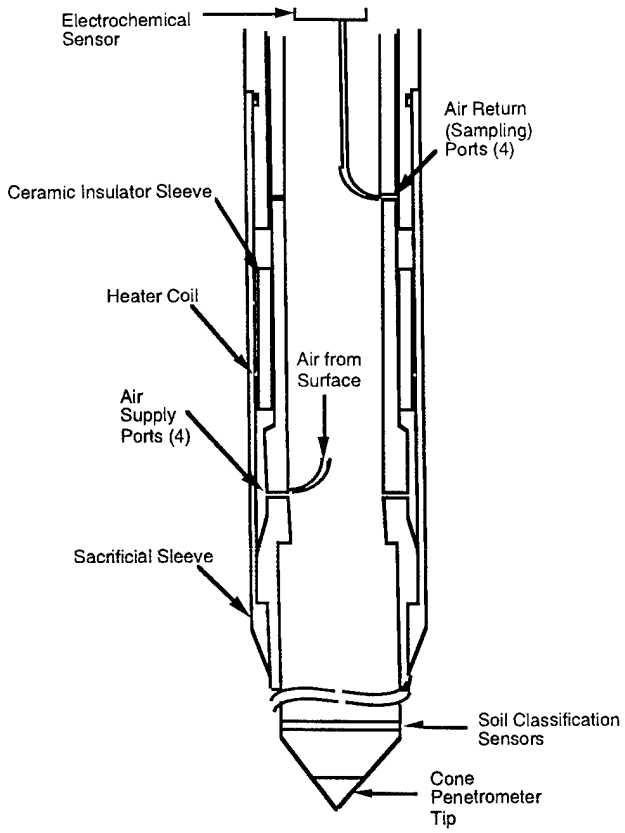

Figure 7. Schematic drawing of pyrolyzer region of the current cone penetrometer explosives probe. Air pumped from the surface passes out through four air supply ports and between the pyrolyzer and heated soil before being drawn back into probe and sent to electrochemical sensor.

is shown in Figure 8, where the infrared diode laser apparatus used to detect NO and NO_2 is the same system used under our WES contract to generate the observations shown in Figure 4.

Our Phase I laser heating experiments were performed in two rounds using two different microchip lasers. In the first round, we used a laser with a 1 W pump which generated only the 1.064 μm fundamental, at an average power level of under 40 mW (the laser we had used earlier to study NO_2 LIF detection sensitivity had generated 532 nm green light as well, and had twice the 1.064 μm power). The experiments involved focusing the laser through a microscope objective, with an inlet tube to the infrared laser/multipass cell NO/NO_2 detection system placed nearby.

We made observations using two types of substrates: 1) a simulated contaminated soil, composed of 1 per cent by weight finely ground TNT in sand, covered with a thin layer of dry New Hampshire soil, and 2) larger single particles of TNT (4-5 mg, and about 0.5 mm in thickness, with larger dimensions in the two directions perpendicular to the laser beam) in a soil matrix. With the first type of substrate, moving the laser spot across the simulated contaminated soil resulted in the observation of occasional spikes of NO with peak concentrations in the 30-100 ppb_v range. Our studies of larger particles of TNT yielded two interesting observations: a) the absorption coefficient of pure TNT for 1.064 μm light is very small, probably under 5 per cent for the 0.5 mm chips, and b) by measuring the volume of the hole evaporated in the TNT crystal and

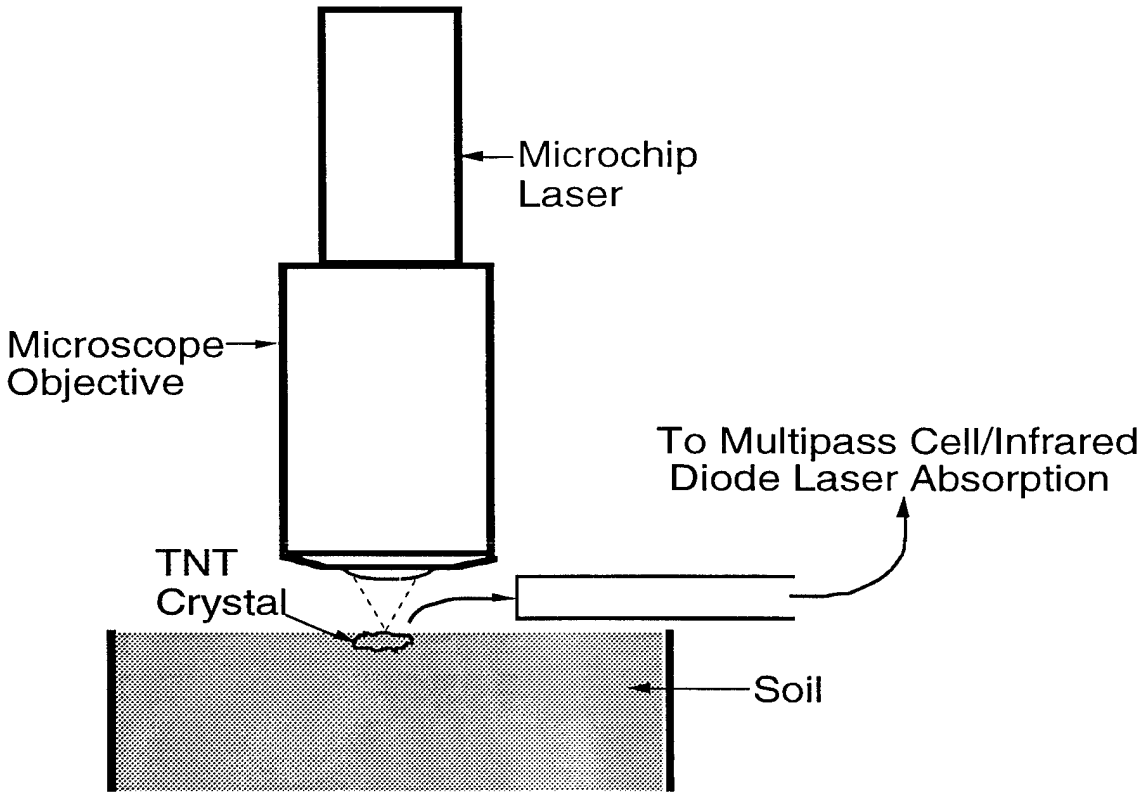

Figure 8. Schematic of First Round of Laser Soil Heating Experiments.

integrating under the NO concentration-versus-time curve, the ratio of (moles of NO sampled) to (moles of TNT evaporated) is found to be remarkably high, in the range of 0.1 to 0.2. Because of the low absorption coefficient, the major heat transfer mechanism is absorbance of infrared laser light by a thin film of soil, followed by conduction heat transfer to the TNT. Calculations using a simple heat transfer model suggest that liquid layer temperatures do not greatly exceed 100 °C. Our previous experiments using TNT particles in small heated tubes have suggested that for short times and low surface temperatures the fraction of NO generated from evaporating TNT should be small. However, we are convinced that the high efficiency of conversion from TNT to NO in laser heating is a true observation, even if the mechanism will require clarification.

The second round of laser heating experiments still used a microchip laser with a 1 W pump, but now in addition to a 1.064 μm average power level of 20 mW, it had a green (532 nm) average power of 22 mW and an ultraviolet (266 nm) power level of 6 mW. It had been suggested that we might see enhanced conversion of TNT to NO due to ultraviolet photolysis, and the above ultraviolet power level is such that on the order of one photon is input for each TNT molecule evaporated. A simple lens replaced the microscope objective shown in Figure 8 so that the ultraviolet light could be focused along with the green and near infrared light. Laser heating of 4-5 mg TNT chips resulted in peak NO levels in the 1-2 ppm_v range, where such experiments using the first round laser showed maximum excursions over the background of only 50-150 ppb_v. There are two additional results of this second set of laser heating experiments. First, substantial NO_2 production from TNT chips heated by this laser, in the range of 150-350 ppb_v, were observed. This could be due in part to ultraviolet photolysis of TNT. A second additional

observation was that with this laser a thin coating of soil is not required for the production of NO and NO_2 from the TNT. A higher absorption coefficient for green light (our TNT particles are visibly opaque, with a beige color) could lead to this effect.

The role of ultraviolet photolysis on the generation of NO and NO_2 from TNT could be studied by filtering out the uv light. A KCl window, which transmits the green and infrared light of the laser but not the uv light, could be placed in the beam path. With the presently available laser system, however, eliminating the uv (6mW) and a small amount of the ir and visible light in reflection and/or scatter on the window surface, would bring the total power remaining close to or below the threshold for TNT melting. Experiments of this kind would be inconclusive in the determination of the significance to uv photolysis at this time and will therefore be left for Phase II work with a higher power laser .

Even though the above results for large TNT chips were in accord with our expectations of larger signals for this slightly higher power laser, with the possibility of further enhancements due to the presence of green and/or ultraviolet light, when we observed the same 1 per cent by weight finely ground TNT in sand sample as in the first round we saw only 30-40 ppb_v NO excursions above the background level. It is possible that these observations are not significantly different than the 30-100 ppb_v NO range quoted above for the first round, since both rounds of experiments involved few observations with large variances. It is also possible that other systematic changes in the experiment offset the increase in laser power, but such differences have not been identified.

In the second round of laser heating experiments we went on to make observations of a sample of contaminated soil sent to us by WES, collected on 17 October 1996 during their most recent field test at Volunteer Army Ammunition Plant near Chattanooga, TN. This sample had been analyzed at 2237 ppm_w, so a five times lower concentration than the TNT-in-sand simulation sample discussed above. TNT distribution in real soil samples can be very inhomogeneous, but we ground and mixed this sample before the laser heating studies, which we expect substantially improved its homogeneity at the level of laser heating spot sizes. This sample gave in the range of 15-25 ppb_v NO excursions above background levels. In the second round experiments which examined contaminated soil sample or 1% TNT in sand, spikes in NO mixing ratio, as was observed in first round experiments, were not seen. Instead, a general elevation in NO with some additional increases on top of that were observed.

These NO levels from a heavily contaminated real sample are many orders of magnitude smaller than the levels expected from the old 900° C filament heater in the original cone penetrometer probe. However, they are still detectable, in principal, and may be significantly increased when a microchip laser system with a 10 W pump is used. We do not plan to draw any final conclusions about the feasibility of laser heating of soil until we have carried out a comprehensive series of experiments with the higher power Phase II laser system. Among the issues we must address in Phase II are: 1) What is the physical form of TNT in contaminated soils, and what is the result when TNT contaminations are reduced from our example 1 per cent (wt) to 1 ppm_{wt}; i.e., will the time between spikes increase, or their height or width decrease, or some combination of all of these? 2) Is the observed sensitivity limit of the current sensor determined by its noise level or by background NO fluctuations? 3) How can we ensure proper positioning of heating laser focus and air sampling intake relative to the soil surface, in ways which will not be obscured and clogged? Our first observations of laser heating seem to hold some promise, but its is clear that much work remains to be done.

3. List of Publications and Technical Reports

This Phase I final report and 11 monthly technical reports are the only reports submitted to ARO under the program. To date, no publications have been submitted under the program.

Several oral presentations have been made which included discussion of various aspects of this program. On 21 March, 1996, J. Wormhoudt of ARI gave a talk at the 1996 Laser Applications to Chemical and Environmental Analysis Topical Meeting of the Optical Society of America, with the title "Advanced Laser Detection Techniques for Cone Penetrometer Sensors", which included an introduction to the techniques and goals of the project. On 23 July, 1996, J. Wormhoudt made a presentation at the Geotechnical Laboratory of the U. S. Army Engineer Waterways Experiment Station (WES), during an ARO Principal Investigators site visit, presenting the goals and planned work for the project. And on 24 October, 1996, J. Wormhoudt gave an invited talk at the Optical Society annual meeting in Rochester, NY, which focused on the studies of laser heating of contaminated soils begun near the end of the Phase I program.

4. List of Inventions

No inventions were made under this program.

5. List of All Participating Scientific Personnel

Participating scientific personnel included J. H. Shorter, J. Wormhoudt and C. E. Kolb at Aerodyne Research and J. J. Zayhowski, B. Johnson and N. Newbury at MIT Lincoln Laboratory. No degrees were awarded as part of work on the program.

6. Bibliography

Bowders, J.J. and Dansel, D.T, 1994, "Summary Report at The Workshop on Advancing Technology for Cone Penetrometer Testing of Geotechnical and Geoenvironmental Site Characterization," June 1994, University Texas, Austin, TX.

Boyd, G.D., Ashkin, A., Dziedzic, J.M., Klein, D.A., 1965, Phys. Rev. A 137, 1305.

Cespedes, E.R., Cooper, S.S., Davis, W.M., Buttner, W.J., and Vickers, W.C., 1995, "In Situ Detection of TNT Contamination Using Electrochemical Sensors in Cone Penetrometer System," in Optical Sensing for Environmental and Process Monitoring 1, Proc. SPIE 2367, pp. 33-42.

Cespedes, E.R., Miles, B.H., and Lieberman, S.H., 1994, "Development of Optical Sensors for the Site Characterization and Analysis Penetrometer System (SCAPS)," in Optical Sensing for Environmental Monitoring, Air and Waste Management Association SP89, pp. 621-632.

Davis, W.M., 1995, "WES Cone Penetrometer Program and Sensor Requirements," Presented to the ARO Chemistry Review Panel, January 1995, Research Triangle Park, NC.

Eckardt, R.C., Masuda, H., Fan, Y.X., and Byer, R.L., 1990, IEEE J. Quantum Electron. 26, 922.

Patten, Jr., K. O., Burley J. D., and Johnston, H. S., 1990, "Radiative Lifetimes of Nitrogen Dioxide for Excitation Wavelengths from 400 to 750 nm," J. Phys. Chem. 94, 7960.

Schofield, K., 1977, "Atomic and Molecular Fluorescence as a Stratospheric Species Monitor," J. Quant. Spectrosc. Radiat. Transfer 17, 13.

Szabo, A.and Stein, R. A., 1965, J. Appl. Phys. 36, 1562.

Wormhoudt, J., Shorter, J.H., McManus, J. B., Kebabian, P. L., Zahniser, M. S., Davis, W. M., Cespedes, E. R. and Kolb, C. E., 1996, "Tunable Infrared Laser Detection of Pyrolysis Products of Explosives in Soils," Appl. Opt. 35. 3992 (1996).

Zayhowski, J. J. and Dill, III, C., 1994, "Diode-Pumped Passively Q-Switched Picosecond Microchip Lasers", Opt. Lett. 19, 1427.

Zayhowski, J.J., Ochoa, J., and Dill, C. III., 1995, "UV Generation with passively Q-switched picosecond microchip lasers," in Conference on Lasers and Electro-Optics, 1995 Technical Digest Series, Vol. 9 (Optical Society of America, Baltimore, Maryland, 21-26, 1995) p. 139.

Zayhowski, J. J., 1995, Patent No. 5,394,413, February 28, 1995.

Zayhowski, J. J. and Kelley, P. L., 1991, IEEE J. Quantum Electron. 27, 2220.

Zayhowski, J. J. and Kelley, P. L., 1993, IEEE J. Quantum Electron, 29, 1239.

Zayhowski, J. J., 1996, "Ultraviolet generation with passively Q-switched microchip lasers," Opt. Lett. 21, 588.